Graph-time spectral analysis for atrial fibrillation

Sun, Miao; Isufi, Elvin; de Groot, Natasja M.S.; Hendriks, Richard C.

DOI
10.1016/j.bspc.2020.101915

Publication date
2020

Document Version
Accepted author manuscript

Published in
Biomedical Signal Processing and Control

Graph-Time Spectral Analysis for Atrial Fibrillation

Miao Sun[a,*], Elvin Isufi[a], Natasja M.S. de Groot[b] and Richard C. Hendriks[a]

[a]Faculty of Electrical Engineering, Mathematics and Computer Science, Delft University of Technology, The Netherlands.
[b]Department of Cardiology, Erasmus University Medical Center, The Netherlands.

ARTICLE INFO

Keywords:
Atrial fibrillation
Graph signal processing
Spectral analysis
Atrial activity extraction
Graph-time signal processing

Abstract

Atrial fibrillation is a clinical arrhythmia with multifactorial mechanisms still unresolved. Time-frequency analysis of epicardial electrograms has been investigated to study atrial fibrillation. However, deeper understanding can be achieved by incorporating the spatial dimension. Unfortunately, the physical models describing the spatial relations of atrial fibrillation signals are complex and non-linear; hence, conventional signal processing techniques to study electrograms in the joint space, time, and frequency domain are less suitable. In this study, we wish to put forward a radically different approach to analyze atrial fibrillation with a higher-level model. This approach relies on graph signal processing to represent the spatial relations between epicardial electrograms. To capture the frequency content along both the time and graph domain, we propose the joint graph and short-time Fourier transform. The latter allows us to analyze the spatial variability of the electrogram temporal frequencies. With this technique, we found the spatial variation of the atrial electrograms decreases during atrial fibrillation since the high temporal frequencies of the atrial waves reduce. The proposed analysis further confirms that the ventricular activity is smoother over the atrial area compared with the atrial activity. Besides using the proposed graph-time analysis to conduct a first study on atrial fibrillation, we demonstrate its potential by applying it to the cancellation of ventricular activity from the atrial electrograms. Experimental results on simulated and real data further corroborate our findings in this atrial fibrillation study.

1. Introduction

Atrial fibrillation is a cardiac arrhythmia characterized by rapid and irregular atrial beating and it is correlated with stroke and sudden death [1–3]. Yet, the mechanisms underlying atrial fibrillation remain unresolved and challenging to model. To analyze the disease, different signal processing methods have been applied to the non-invasive body surface electrocardiograms (ECGs), or to the invasive epicardial or endocardial electrograms [4–8]. The epicardial electrogram (EGM) is measured on the heart's surface through multiple electrodes and has a higher spatial resolution compared with ECGs. This improved resolution makes EGMs appealing to analyze atrial fibrillation over both space (heart surface) and time. The methods proposed in the current work concern EGM data.

Although different studies have analyzed electrograms data in time and frequency domain [9–13], there remain many open questions that require alternative and novel tools to investigate atrial fibrillation. Experience in signal processing suggests that incorporating the spatial dimension into the time-frequency analysis may yield improved insights on the atrial activity. However, the physical models for spatial propagation are relatively complex and non-linear; hence, rendering conventional signal processing methods are less suitable for a joint space, time, and frequency domain analysis [14, 15]. It is also difficult to use physical models for extracting useful information, e.g., activation time or conductivity [16].

In this work, we wish to suggest a novel approach to model epicardial electrograms at a higher abstraction level. This approach represents the spatial relation of different epicardial electrograms through a graph and relies on graph signal processing to investigate electrograms in the joint space, time, and frequency domain. We conduct a first study with the proposed framework to identify spectral differences between sinus rhythm (normal heart rhythm) and atrial fibrillation, and between atrial and ventricular activities. We also leveraged the proposed graph model to remove ventricular components from the raw EGM measurements.

Graph-time signal processing: Graphs are natural tools to model data living in high-dimensional and irregular domains [17]. Graph signal processing provides a harmonic analysis for signals residing on the graph vertices and has been applied to brain signal analysis, Alzheimer classification, and body motion [18–24]. However, despite showing promise, graph signal processing is still unexplored for heart-related problems. The EGM signals considered in this work are (spatially) high-dimensional measurements taken from epicardial sites of the atria during open-heart surgery [25]. Graph signal processing poses itself then as a valid candidate to account for the underlying mechanisms for analyzing atrial fibrillation. The atrial activity during atrial fibrillation is a complicated process for which it is hard to find a good and tractable mathematical model. Graph signal processing can tackle this issue by formulating a high-level model for the atrial activity; hence, taking a step further towards exploring the atrial fibrillation behavior. The use of graphs to understand atrial fibrillation has also been considered in [26]. This work explored the association between different atrial regions through basic graph theory (e.g., graph topology, density, average degree), yet left unexplored the processing of signals on top of this graph. Instead, we here investigate EGMs through graph signal processing.

*Corresponding author
Email address: M.Sun@tudelft.nl (Miao Sun)

The predominant tool in graph signal processing is the graph Fourier transform; a generalization of the temporal Fourier transform that provides a frequency interpretation for graph data. Similar to the time domain, the graph frequency components characterize the signal variation, now, over the graph and have shown to be useful to study biological activities [18–20]. However, since the EGM varies with time, it is insufficient to consider the graph Fourier transform alone as it analyzes the spatial variability for a fixed time instant. To account for the temporal variability and capture the interaction between space and time, we can consider the so-called product graphs [27]. A conceptual simpler alternative is to apply the graph Fourier transform on the data after applying the temporal Fourier transform (which tends to decorrelate the time-domain data). Since the electrogram is non-stationary, we use a joint graph and short-time Fourier transform to investigate the spatial properties of the temporal frequency content in a short-time period. Compared with the product graph method, working on the joint graph-time domain is simpler, and the analysis can be done independently per temporal frequency.

Spectral EGM analysis: We apply the graph-time spectral analysis to characterize the spectral properties of the EGMs in the graph and time domain. We first evaluate the spatial variation of the EGMs at different temporal frequencies during sinus rhythm and atrial fibrillation. During atrial fibrillation, we show the high temporal frequencies of the atrial activity reduce, leading to a decrease of the spatial variation. We also observed the spatial variation of the atrial activity is higher than the spatial variation of the ventricular activity. We used this difference in behavior to extract the atrial activity from the mixed EGM measurement.

Atrial activity extraction: Electrograms measured on the atrial sites are naturally corrupted by the ventricular activity. The capability of a method to extract the atrial activity is fundamental to promote it for atrial fibrillation studies. A common technique to extract the atrial activity is template matching such as average beat subtraction [28]. However, this simple method does not adapt to changes in the EGM morphology caused by the variations in the heart activities. To deal with this shortcoming, adaptive ventricular cancellation [29] has been proposed to extract the atrial activity. Nevertheless, its performance is unstable as it relies on the reference signal, often obtained with a reference lead. Another class of techniques using multi-lead information are the signal separation algorithms such as principal component analysis [30] and independent component analysis [31]. Results of these methods are compared in [32]. However, it is questionable whether the statistical assumptions made by these methods for ECGs (e.g. on the distribution and independence of components) still hold for epicardial data. Motivated by our spectral analysis of the ventricular activity, we proposed a more effective algorithm for atrial activity extraction based on graph signal smoothness. Our method captures the morphology in the heart activities and does not require uncorrelated or independent assumption between leads. Our numerical results on both synthetic and real data confirm the potential of graph-based atrial extraction algorithm over comparative alternatives. The latter corroborate the graph-time spectral insights for atrial fibrillation.

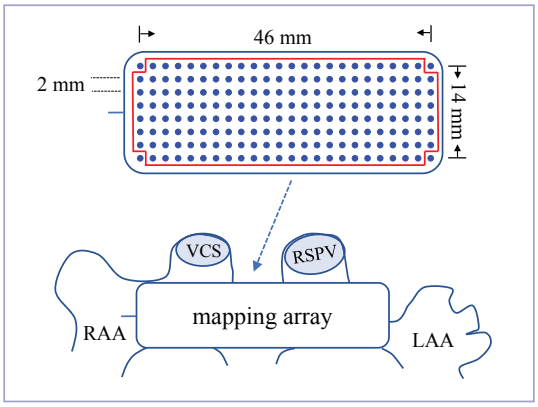

Figure 1: Mapping array and its placement on the Bachmann's bundle area of the atria [25]. RAA: right atrial appendage; LAA: left atrial appendage; VCS: vena cava superior; RSPV: right superior pulmonary vein.

Contribution and organization: Altogether, this paper puts forward a radically different approach to analyze the epicardial electrograms from a higher abstraction level. This approach relies on graph signal processing and reveals features of biological and engineering interest. It also shows promise to remove interference from the atrial electrogram. More concretely, the contributions of this paper are: (i) To propose a high-level graph signal processing model for analyzing the epicardial electrogram; (ii) To evaluate the temporal and spatial variation of epicardial electrograms with a graph-time spectral analysis framework. This helps to: (ii-a) recognize atrial fibrillation impact on the atrial activity; (ii-b) identify differences between the atrial and ventricular activities; (iii) To propose a novel and effective atrial activity extraction algorithm based on the graph-time variations of the atrial and ventricular activities.

The rest of this paper is organized as follows. Section 2 describes the data used in this work. Section 3 introduces the basic notions of graph signal processing and the joint graph and short-time Fourier transform. Section 4 performs the graph-time spectral analysis under sinus rhythm and atrial fibrillation. Section 5 introduces the graph-based atrial activity extraction algorithm and Section 6 evaluates its performance on synthetic and real data. We discuss the paper contributions and future directions in Section 7 and draw the conclusions in Section 8.

2. Database

We used the epicardial electrogram data measured on human atria during open-heart surgery as reported in [25]. Ten patients (aged 64±16; 20% female) are analyzed in this study. Three patients underwent surgery due to aorta ascendens dilatation and the remaining seven due to aortic valve and coronary artery disease; all patients did not have a re-

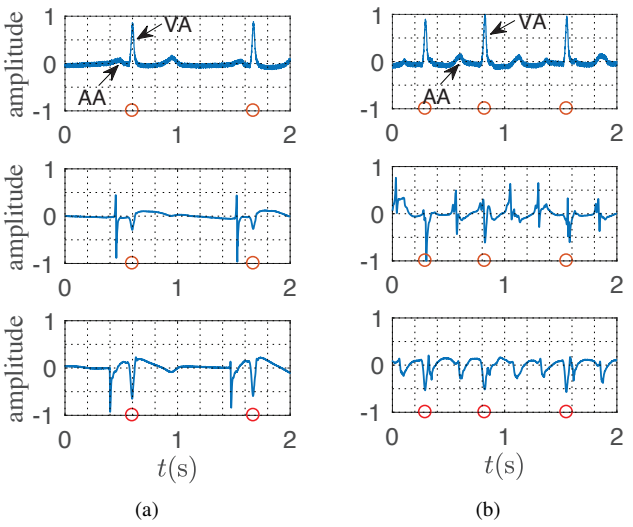

Figure 2: Examples of the body surface electrocardiogram (ECG) and epicardial electrogram (EGM) across time at one electrode during (a) sinus rhythm and (b) atrial fibrillation. AA: atrial activity; VA: ventricular activity. *Top*: ECG; *middle* and *bottom*: EGMs at different electrodes. The red circles mark the peak of the ventricular activity determined by the ECG measurements.

ported history of atrial fibrillation. The atrial fibrillation was induced manually by rapid pacing in the right atrial free wall with the procedure detailed in the original publication [25]. We remark that induced atrial fibrillation has also been used to investigate the disease in [26] and [9]. For each patient, both sinus rhythm and atrial fibrillation data are recorded.

Previous research has suggested the Bachmann's bundle area is related to the pathophysiology of atrial fibrillation [33]. However, this area is still one of the less understood. Because of the connection with atrial fibrillation and the interesting research aspects, we will hereinafter focus on the EGMs measured on the Bachmann's bundle.

A mapping array of 8×24 electrodes with an inter-electrode distance of 2 mm is used to collect data. During the measurement phase, 188 electrodes record the EGMs; these are the electrodes in the red box in Figure 1. Three of the remaining electrodes record the body surface ECG signal, the reference signal, and the calibration signal, respectively; the last electrode is not used. The electrogram comprises five seconds of recordings during sinus rhythm and ten seconds during atrial fibrillation with a sampling rate of 1 kHz. All measurements were taken in the Erasmus Medical Center, The Netherlands, during 2014-2016 with procedures approved by the Medical Ethical Committee (MEC 2010-054 & MEC 2014-393) [34, 35]. Further details about the data acquisition system are reported in [25].

Figure 2 illustrates the ECGs and the EGMs during sinus rhythm and atrial fibrillation for one patient. In the ECG (top plots in Figures 2(a) and 2(b)), the high peaks indicate the ventricular activity, while the lower peaks before them indicate the atrial activity. The atrial activity appears weak compared with the ventricular activity. In the EGM measurements (middle and bottom plots in Figures 2(a) and 2(b)), the atrial activity is more pronounced, albeit short in duration. This difference is due to spatial averaging occurring when measuring the atrial signal on the body surface, compared with when measuring it on the epicardium.

From Figure 2(b), we see that during atrial fibrillation the atrial and the ventricular activities are difficult to distinguish since they appear irregular and overlap. In other words, the ventricular activity affects the analysis on the atrial activity; hence, extracting the atrial activity from the measurement is critical for atrial fibrillation research.

The EGMs measured by the different electrodes (middle and bottom plots in Figure 2) show a time delay when measuring the atrial activity in different positions. However, they do not show any obvious time delay when measuring the ventricular activity. This is because the mapping array is close to the atria and far from the ventricle. Also, the amplitudes of the ventricular activity are different at different electrodes due to the propagation attenuation.

The above discussion highlights the limitations of the body surface ECG–the atrial activity in there is weak and gets easily corrupted by noise; hence, rendering the time-frequency analysis unreliable. Although proposed invasive methods measured a stronger atrial activity, they used low-resolution mapping arrays and analyzed the data only in time or temporal frequency domain [4–7]. Differently, we consider high-resolution epicardial measurements and analyze the data in the joint space, time, and frequency domain.

3. Theory

In this section, we recall the basic concepts on graph signal processing and introduce the joint graph and short-time Fourier transform.

3.1. Graph signal processing

Graphs and graph signals: Consider a network represented by an undirected graph $\mathcal{G} = (\mathcal{V}, \mathcal{E}, \mathbf{W})$, where $\mathcal{V} = (v_1, \cdots, v_K)$ is the set of K vertices, $\mathcal{E}$ is the set of edges, and $\mathbf{W}$ is the graph adjacency matrix with entries $\mathbf{W}(i,j) = W_{i,j}$. Here, $W_{i,j} \geq 0$ represents the edge weight connecting vertices v_i and v_j and $W_{i,j} = 0$ indicates no connection between vertices. The neighbor set of vertex v_i is denoted as $\mathcal{N}_i$. The graph Laplacian matrix is $\mathbf{L} = \mathbf{D} - \mathbf{W}$, where $\mathbf{D}$ is the diagonal degree matrix with $D_{i,i} = \sum_{j=1}^{K} W_{i,j}$.

A graph signal is a set of values over the vertices, i.e., it is a mapping from the vertex set to the set of real numbers, $y : \mathcal{V} \to \mathbb{R}$. The epicardial electrograms recorded by all electrodes in the mapping array is an example of a graph signal. Let $y_i(t)$ be the signal of vertex v_i at time t for $i = 1, \ldots, K$ and $t = 0, \ldots, T-1$. The graph signal at time t is compactly represented by the $K \times 1$ vector $\mathbf{y}(t) = [y_1(t), y_2(t), \ldots, y_K(t)]^T$.

The electrical activities recorded by the electrodes are related to each other and form an electrical network. We constructed a graph by considering each electrode as a vertex. There are two ways to build the edges in the graph: (i)

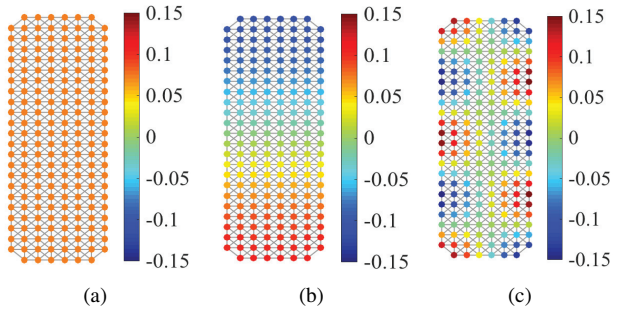

Figure 3: Different graph Laplacian eigenvectors of the graph. (a) $\mathbf{u}_0 = 1/\sqrt{K}\mathbf{1}$ is the constant eigenvector shown by the same color over all vertices; (b) $\mathbf{u}_1$ is a slow-varying eigenvector shown by a smooth color transition from the top vertices to the bottom ones; (c) $\mathbf{u}_9$ is a faster-varying eigenvector over the graph shown by the multiple color variations in adjacent vertices.

based on the data structure, e.g., correlation; (ii) based on physical properties, e.g., distance.

To compare the sinus rhythm signal with the atrial fibrillation signal, we consider a fixed graph structure for both situations. With the illustration in Figure 3(a), the edges are determined by the electrodes position; each vertex is connected with its eight nearest neighbors. This expresses that an electrode (vertex) has strong similarities with the surrounding electrodes. In other words, this graph is built with the prior knowledge that under healthy conditions neighboring vertices record a similar signal. The edge weights are based on the distance between two vertices. This is a common approach in graph signal processing when there is little prior knowledge about the signal. The weight of edge $W_{i,j}$ is

$$W_{i,j} = \left(\frac{d_{i,j}}{\alpha}\right)^{-1} \tag{1}$$

where $d_{i,j}$ is the distance between two connected vertices and α is a scaling parameter. We chose α as the smallest distance between two vertices to normalize the largest weight to one.

Graph Fourier transform and smoothness: The graph Laplacian matrix is symmetric, positive semidefinite, and accepts the eigenvalue decomposition

$$\mathbf{L} = \mathbf{U}\mathbf{\Lambda}\mathbf{U}^H \tag{2}$$

where $\mathbf{U} = [\mathbf{u}_0, \mathbf{u}_1, \cdots, \mathbf{u}_{K-1}]$ is the set of orthonormal eigenvectors, $\mathbf{\Lambda}$ is the diagonal matrix of eigenvalues, and $(\cdot)^H$ is the Hermitian operator. The eigenvalues are sorted in increasing order $0 = \lambda_0 < \lambda_1 \leq \cdots \leq \lambda_{K-1}$.

The graph Fourier transform (GFT) of signal $\mathbf{y}(t)$ with respect to Laplacian $\mathbf{L}$ is

$$\widetilde{\mathbf{y}}(t) = \mathbf{U}^H\mathbf{y}(t) \tag{3}$$

where $\widetilde{\mathbf{y}}(t) = [\widetilde{y}(0,t), \widetilde{y}(1,t), \ldots, \widetilde{y}(K-1,t)]^H$ contains the GFT coefficients $\widetilde{y}(k,t)$ for graph frequency index k of time t. The inverse GFT is

$$\mathbf{y}(t) = \mathbf{U}\widetilde{\mathbf{y}}(t). \tag{4}$$

The GFT generalizes the temporal Fourier transform: for the graph being a cycle that represents the temporal axis of a periodic signal, the GFT matches the discrete Fourier transform [27]. The GFT analyzes the signal variation over the graph for a fixed time instant. Since the transform (eigenvector) matrix $\mathbf{U}$ depends on the graph structure, it gives a harmonic decomposition for signals living in irregular domains where the traditional discrete Fourier transform cannot be applied. For readers familiar with spectral network theory, the GFT can also be seen as the signal projection onto the Laplacian eigenspace.

The GFT coefficients $\widetilde{y}(k,t)$ for lower values of k indicate how much the slower varying eigenvectors over the graph contribute to $\mathbf{y}(t)$. For larger values of k, these coefficients indicate how much the faster varying eigenvectors over the graph contribute to $\mathbf{y}(t)$. The coefficient $\widetilde{y}(0,t)$ indicates the contribution of the constant component (equal to $1/\sqrt{K}$ at each vertex) on $\mathbf{y}(t)$ [36]. Therefore, index k is called the graph frequency index. Figure 3 depicts three eigenvectors of the considered graph: the eigenvector $\mathbf{u}_k$ changes more rapidly over adjacent vertices for larger k.

Just like temporal bandlimited signals, we can define bandlimited graph signals. In many practical cases, the coefficients $\widetilde{y}(k,t)$ have only a few non-zero entries. A bandlimited graph signal $\mathbf{y}(t)$ is therefore defined as a graph signal with GFT coefficients [36]

$$\widetilde{y}(k,t) = 0, \text{ for } k > K_0 \in \{0, \cdots, K-1\} \tag{5}$$

implying the signal has no content outside the graph frequency band of $\{0, K_0\}$. In this study, we will often see that EGM signals exhibit a bandlimited behavior over the graph.

To measure the signal variation over the graph, the graph Laplacian quadratic form of $\mathbf{y}(t)$ is defined as [36]

$$\begin{aligned} \mathrm{V}_{\mathcal{G}}(\mathbf{y}(t)) &= \mathbf{y}(t)^H\mathbf{L}\mathbf{y}(t) \\ &= \sum_{i\in\mathcal{V}}\sum_{j\in\mathcal{N}_i} W_{i,j}\,(y(i,t) - y(j,t))^2. \end{aligned} \tag{6}$$

This quadratic form shows the variation of signal $\mathbf{y}(t)$ over the vertices for a fixed t is a weighted sum of the difference between any two connected vertices. The edge weight indicates the contribution of a connection to the overall variation. If $\mathrm{V}_{\mathcal{G}}(\mathbf{y}(t))$ is small, the signal is smooth, i.e., it has similar values in adjacent vertices. If $\mathrm{V}_{\mathcal{G}}$ is large, the signal changes faster over the graph, i.e., it has different values in adjacent vertices. For the three eigenvector signals in Figure 3, we have $0 = \mathrm{V}_{\mathcal{G}}(\mathbf{u}_0) < \mathrm{V}_{\mathcal{G}}(\mathbf{u}_1) < \mathrm{V}_{\mathcal{G}}(\mathbf{u}_9)$.

3.2. Joint STFT and GFT

Graph signal processing considers only a single time instant and does not capture the correlation across time. Since the signals we study are time-varying and non-stationary, the

joint graph and short-time Fourier transform is defined next to exploit signal dependencies across both graph and time. In simple words, the short-time Fourier transform (STFT) is applied first to transform the signal per vertex to the temporal frequency domain; this approximately decorrelates the data per vertex. Subsequently, the GFT is applied to each temporal frequency to treat each frequency as an independent graph signal.

Let us split the signal into M temporal frames of length T_M and let $\mathbf{y}(\tau, t) \in \mathbb{R}^{K\times 1}$ be the graph signal in frame $\tau \in \{0, \dots, M-1\}$ at time instant t, i.e., the signal of all electrodes at one time instant. We collect all signals recorded in frame τ in the matrix

$$\mathbf{Y}(\tau) = [\mathbf{y}(\tau, \tau T_M), \mathbf{y}(\tau, \tau T_M + 1), \cdots, \mathbf{y}(\tau, (\tau+1)T_M - 1)] \in \mathbb{R}^{K\times T_M} \quad (7)$$

where the ith row of $\mathbf{Y}(\tau)$ corresponds to the time-varying signal measured by the ith electrode in frame τ.

For the STFT transform, we consider F temporal frequency bins and apply a temporal window followed the discrete temporal Fourier transform to each row of $\mathbf{Y}(\tau)$. The STFT coefficient matrix of (7) at frame τ over the F temporal frequencies is

$$\hat{\mathbf{Y}}(\tau) = [\hat{\mathbf{y}}(\tau, 0), \hat{\mathbf{y}}(\tau, 1), \dots, \hat{\mathbf{y}}(\tau, F-1)] \in \mathbb{C}^{K\times F} \quad (8)$$

The fth column of $\hat{\mathbf{Y}}(\tau)$ with $f \in \{0, ..., F-1\}$ represents the temporal frequency components of all vertices in frame τ and frequency bin f and is given by

$$\hat{\mathbf{y}}(\tau, f) = \left[\hat{Y}_1(\tau, f), \hat{Y}_2(\tau, f), \cdots, \hat{Y}_K(\tau, f)\right]^H \in \mathbb{C}^K. \quad (9)$$

The GFT is then applied to each column $\hat{\mathbf{y}}(\tau, f)$ of $\hat{\mathbf{Y}}(\tau)$ separately to achieve the joint STFT and GFT matrix

$$\widetilde{\mathbf{Y}}(\tau) = \mathbf{U}^H \hat{\mathbf{Y}}(\tau) \quad (10)$$

with $\widetilde{\mathbf{y}}(\tau, t)$ being the GFT of the temporal frequency signal $\hat{\mathbf{y}}(\tau, f)$; the kth element $\widetilde{y}(k, \tau, f)$ corresponds to the graph frequency index k. For a low value of k, this coefficient indicates how much the slowly varying graph component contributes to the temporal frequency f in time frame τ. Therefore, the joint coefficient quantifies the variation over the graph of a temporal frequency in a short-time period. In other words, each coefficient indicates the EGM variation over space and time. These values will be different when analyzed, for instance, during sinus rhythm compared with atrial fibrillation and they will reveal patterns of space-time variability about the disease.

To obtain again the time-vertex signal $\mathbf{Y}(\tau)$ [cf. (7)] from the joint transform representations, we first apply the inverse GFT to $\widetilde{\mathbf{Y}}(\tau)$ as

$$\hat{\mathbf{Y}}(\tau) = \mathbf{U}\widetilde{\mathbf{Y}}(\tau) \quad (11)$$

to get the STFT matrix $\hat{\mathbf{Y}}(\tau)$. Then, we apply the inverse STFT with overlap-adding to reconstruct the entire time domain signal from the segmented frames.

Similar to (6), the variation of the temporal frequency components $\hat{\mathbf{y}}(\tau, f)$ over the graph can be quantified by the Laplacian quadratic form

$$\begin{aligned} \mathrm{V}_{\mathcal{G}}(\hat{\mathbf{y}}(\tau, f)) &= \hat{\mathbf{y}}(\tau, f)^H \mathbf{L}\hat{\mathbf{y}}(\tau, f) \\ &= \sum_{i\in\mathcal{V}} \sum_{j\in\mathcal{N}_i} W_{i,j}(\hat{Y}_i(\tau, f) - \hat{Y}_j(\tau, f))^2. \end{aligned} \quad (12)$$

The measure in (12) quantifies the graph variation of each temporal frequency f in time frame τ. Since the variation differs in different temporal frequencies, we consider the normalized variation

$$\mathrm{V}_{\mathcal{G},\mathrm{n}}(\hat{\mathbf{y}}(\tau, f)) = \frac{\hat{\mathbf{y}}(\tau, f)^H \mathbf{L}\hat{\mathbf{y}}(\tau, f)}{\hat{\mathbf{y}}(\tau, f)^H \hat{\mathbf{y}}(\tau, f)}. \quad (13)$$

We will in the sequel use this joint transform to analyze the EGMs in three domains: the time domain, the temporal frequency domain, and the graph frequency domain.

4. Graph-time spectral analysis

In this section, we perform a spectral analysis on the EGMs during both sinus rhythm and atrial fibrillation. We first conduct a separate analysis on the short-time Fourier transform and a separate analysis on the graph Fourier transform. Next, in Section 4.2, we conduct a joint transform analysis. As the individual STFT analysis and GFT analysis are of less importance for the remainder of this paper, we only present the main results of the individual STFT and GFT analyses. More details can be found in the supplementary materials.

4.1. STFT analysis & GFT analysis

For the STFT analysis, we analyzed the distribution of the signal energy across both time and temporal frequencies. We observed the atrial activity has wider frequency bandwidth than the ventricular activity. This implies the atrial activity varies faster across time than the ventricular activity. We also found the atrial activity during sinus rhythm has more energy in higher temporal frequencies than during atrial fibrillation. This suggests atrial fibrillation reduces the high temporal frequencies of the atrial waves.

In the GFT analysis, we found the atrial activity varies faster over the graph than the ventricular activity. We also observed the EGM has a larger graph bandwidth during sinus rhythm than during atrial fibrillation. That is, the signal changes faster across the graph (hence epicardium) during sinus rhythm than during atrial fibrillation.

However, we may expect a higher spatial variation of the atrial activity during atrial fibrillation than during sinus rhythm. This is because the signal changes more frequently across time during atrial fibrillation. To explain this counter-intuitive result in the GFT analysis, we need to exploit the association between the temporal and spatial variations. Since the temporal frequencies provide additional insights on the EGMs and since the GFT alone does not capture them, we analyze next the EGMs with the joint STFT and GFT to address the latter.

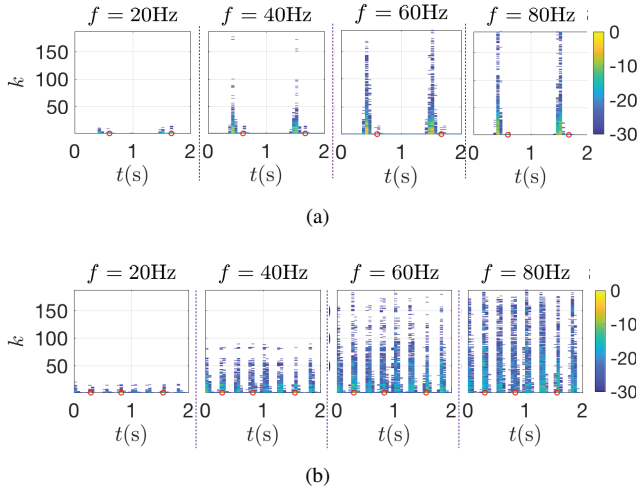

Figure 4: Normalized energy in dB in the joint graph and short-time Fourier transform domain. (a) sinus rhythm; (b) atrial fibrillation. The scalar k represents the graph frequency index, $t(s)$ the time in seconds, and f the temporal frequency. Each plot shows the spatial distribution of the signal energy as a function of time; different plots refer to different temporal frequencies. The red circles mark the peak of the ventricular activity.

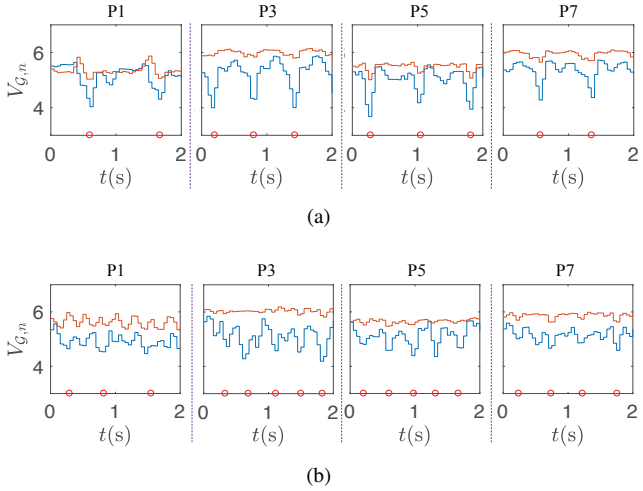

Figure 5: Smoothness measure over time of the low and high temporal frequencies in the joint graph and short-time Fourier transform domain. (a) sinus rhythm; (b) atrial fibrillation. The red and blue lines indicate the mean smoothness of the low and high temporal frequencies, respectively. The red circles mark the peak of the ventricular activity.

4.2. Joint STFT and GFT analysis

In the joint analysis, we analyzed the normalized signal energy in the joint short-time Fourier transform and graph Fourier transform domain. Figures 4(a) and 4(b) depict the results during sinus rhythm and atrial fibrillation for one patient. To improve visualization, we focus on the temporal frequencies 20 Hz, 40 Hz, 60 Hz, and 80 Hz. Overall, the temporal frequency components change slowly over the graph; this is reflected by the energy concentration in the low graph frequencies. However, we also observed that higher temporal frequencies change faster over the graph compared with the lower ones; this is reflected by the higher energy concentration in the high graph frequencies for $f = 60$ Hz, and 80 Hz.

To quantify the graph spatial variations of the low (0 Hz to 100 Hz) and high (100 Hz to 500 Hz) temporal frequencies, we calculated the average variation following (13). Due to space limitation, we show in Figure 5 the results for four representative patients. We can see the high temporal frequencies have a larger graph variation compared to the lower temporal frequencies. This explains the result in the GFT analysis, i.e., the atrial activity has a higher spatial variation during sinus rhythm than during atrial fibrillation. Because from the STFT analysis, the atrial activity has more energy in the high temporal frequencies during sinus rhythm than during atrial fibrillation. This also suggests that the spatial variation is correlated to the temporal variation. If a signal changes rapidly across time, it will have higher energy in the high temporal frequencies. This high variation across time translates then into a higher variation over the graph.

During sinus rhythm, the spatial variation decreases to a small value when the ventricular activity appears. That is, the temporal frequencies change slower over the atria during the ventricular activity than during the atrial activity. But during atrial fibrillation, the spatial variation during the ventricular rhythm is higher because of the coupling between the atrial and ventricular activities.

The above analysis shows that it is possible to separate the atrial and ventricular activities based on their spatial variations. This separation is infeasible by the STFT alone (which ignores correlation across space) or by the GFT alone (which ignores correlation across time). Since the joint transform analyzes the graph signal in short-time periods, it improves separation of the two activities in the joint domain. In the next section, we will leverage these observations to extract the atrial activity in the joint domain.

5. Graph-Based Atrial Activity Extraction

Recall the atrial activity measurements are often corrupted by ventricular activity. In the sequel, we propose an algorithm to extract the atrial activity from the mixed measurements based on the joint graph-time variation.

The graph-time analysis in Section 4.2 showed the ventricular activity is smoother over the graph than the atrial activity. We, therefore, exploit the difference in smoothness to estimate the ventricular activity from the noisy epicardial measurement. The atrial activity can be then obtained by subtracting the estimated ventricular activity from the EGM.

By considering the EGM as a linear combination of the atrial and the ventricular activities [29], we can write the mixed signal $\mathbf{y}(t)$ over the K electrodes at time t as

$$\mathbf{y}(t) = \mathbf{a}(t) + \mathbf{v}(t) \tag{14}$$

where $\mathbf{a}(t)$ indicates the atrial signal and $\mathbf{v}(t)$ the ventricular signals. By segmenting the signal into overlapping frames,

we represent the signal at frame τ in the matrix form as

$$\mathbf{Y}(\tau) = \mathbf{A}(\tau) + \mathbf{V}(\tau) \tag{15}$$

where $\mathbf{Y}(\tau)$, $\mathbf{A}(\tau)$, and $\mathbf{V}(\tau)$ are $K \times T_M$ matrices following from (7). Then, from the joint STFT and GFT transform we get the joint spectral representation

$$\widetilde{\mathbf{Y}}(\tau) = \widetilde{\mathbf{A}}(\tau) + \widetilde{\mathbf{V}}(\tau) \tag{16}$$

where $\widetilde{\mathbf{Y}}(\tau)$, $\widetilde{\mathbf{A}}(\tau)$, and $\widetilde{\mathbf{V}}(\tau)$ are the joint transforms of the mixed EGM signal, atrial activity, and ventricular activity, respectively. The respective columns are $\widetilde{\mathbf{y}}(\tau, f)$, $\widetilde{\mathbf{a}}(\tau, f)$, and $\widetilde{\mathbf{v}}(\tau, f)$.

Since the ventricular activity $\widetilde{\mathbf{v}}(\tau, f)$ is smoother over the graph than the atrial activity $\widetilde{\mathbf{a}}(\tau, f)$, we estimate $\widetilde{\mathbf{v}}(\tau, f)$ as a smooth graph signal reconstruction with minimum distortion from the mixed EGM $\widetilde{\mathbf{y}}(\tau, f)$. This consists of solving the problem

$$\begin{aligned} &\underset{\widetilde{\mathbf{v}}(\tau, f)}{\text{minimize}} \quad ||\widetilde{\mathbf{y}}(\tau, f) - \widetilde{\mathbf{v}}(\tau, f)||_2^2 \\ &\text{subject to} \quad \frac{\widetilde{\mathbf{v}}^H(\tau, f)\mathbf{\Lambda}\widetilde{\mathbf{v}}(\tau, f)}{\widetilde{\mathbf{v}}^H(\tau, f)\widetilde{\mathbf{v}}(\tau, f)} \leqslant c. \end{aligned} \tag{17}$$

where the cost function seeks for finding a ventricular signal $\widetilde{\mathbf{v}}(\tau, f)$ that is close to the EGM measurement $\widetilde{\mathbf{y}}(\tau, f)$, while the constraint imposes the maximum normalized variation to be at most c for all frames τ and temporal frequencies f [cf. (13)].

The ventricular activity estimated from (17) is given by the closed-form expression

$$\widetilde{\mathbf{v}}(\tau, f) = [(1 - \mu c)\mathbf{I} + \mu\mathbf{\Lambda}]^{-1}\widetilde{\mathbf{y}}(\tau, f) \tag{18}$$

where μ is the so-called Lagrangian multiplier (see supplementary materials). After estimating the ventricular activity, we can recover the atrial activity by

$$\widetilde{\mathbf{a}}_{\text{est}}(\tau, f) = \widetilde{\mathbf{y}}(\tau, f) - \widetilde{\mathbf{v}}(\tau, f). \tag{19}$$

Finally, we obtain the time domain signals through the inverse transforms.

The proposed algorithm relies on the presence of the ventricular activity. Since the ventricular activity has most of its energy in the zero graph frequency (see Figure 4), we can detect it by thresholding the signal energy in the joint STFT and GFT domain. If the energy in the zero graph frequency index ($k = 0$) exceeds this threshold, it indicates the presence of the ventricular activity. We can see that the graph-time spectral analysis provides us new insights into the atrial and the ventricular activities, which help to detect and cancel the ventricular activity from measurements.

6. Evaluation of Atrial Activity Extraction

To evaluate the performance of the proposed graph-based atrial activity extraction (GAE) algorithm, we need the ground truth pure atrial activity. However, this is unknown for real measurements; hence, we first evaluate the GAE algorithm with synthetic signals and then perform additional experiments with real EGMs. We compared the GAE algorithm with three popular alternatives: average beat subtraction (ABS) [28]; adaptive ventricular cancellation (AVC) [29]; and independent component analysis (ICA) [29].

6.1. Synthetic data generation

There exists several methods to simulate the atrial activity, see e.g., [37–40]. These algorithms simulate well the electrogram during sinus rhythm, but face difficulties during atrial fibrillation. This is because of the overlap between the atrial and the ventricular activities. Also, these methods are more suitable to generate body surface ECGs rather than EGMs. The work in [41] generates atrial EGMs by simulating the activation of the atrial fibers from the movement of a single dipole, which is less realistic. In this work, we focus on the atrial cell level to model the action potential during atrial fibrillation and extend it to the two-dimensional monodomain tissue. The atrial fibrillation is driven by the so-called ectopic foci sources that are located in various points of the tissue. This is one of the standard atrial fibrillation mechanisms in advanced research [42, 43].

The cell action potential follows the Courtemanche model of human atrial cells [44]. To simulate the atrial activity during atrial fibrillation, we reduced the ionic conductance of I_{to} to 50%, I_{Kur} to 50% and I_{CaL} to 30% [45]. This is based on the experimental study of chronic atrial fibrillation in [45]. After generating the signal at the cell level, we used the reaction-diffusion equation to simulate the propagation of the action potential along the tissue [46]. The diffusion equation is given by

$$C_{\text{m}}\frac{\partial V_{\text{m}}}{\partial t} = I_{\text{tm}} + I_{\text{stim}} - I_{\text{ion}} \tag{20}$$

where V_{m} is the transmembrane potential, $C_{\text{m}} = 100$ pF is the transmembrane capacitance, I_{ion} is the total ionic current calculated from the Courtemanche model, I_{stim} is the stimulus current, and I_{tm} is the transmembrane current. The latter is calculated as

$$I_{\text{tm}} = \frac{1}{S_v}\nabla \cdot (\mathbf{D}\nabla V_{\text{m}}) \tag{21}$$

where S_v is the surface-to-volume ratio, $\nabla(\cdot)$ is the partial derivative operator, and $\mathbf{D}$ is the conductivity tensor.

We considered a two-dimensional tissue of 200×200 cells with a cell radius of 5 μm. The longitudinal conductivity is 1.1 mS cm^{-1}. The transversal to longitudinal conductivity ratio is one-to-two. We discretized the model through finite differences with 0.01 cm spatial resolution and solved the reaction-diffusion equation [cf. (20)] with the Euler method with a time step of 0.05 ms. Five ectopic foci sources drove the irregular atrial activity as illustrated in Figure 6. We applied stimuli of 50 ms in length on these positions. Two atrial cycle length of 160 ms and 180 ms were used to simulate different degrees of atrial fibrillation. For each type, we generated six segments of 10s each.

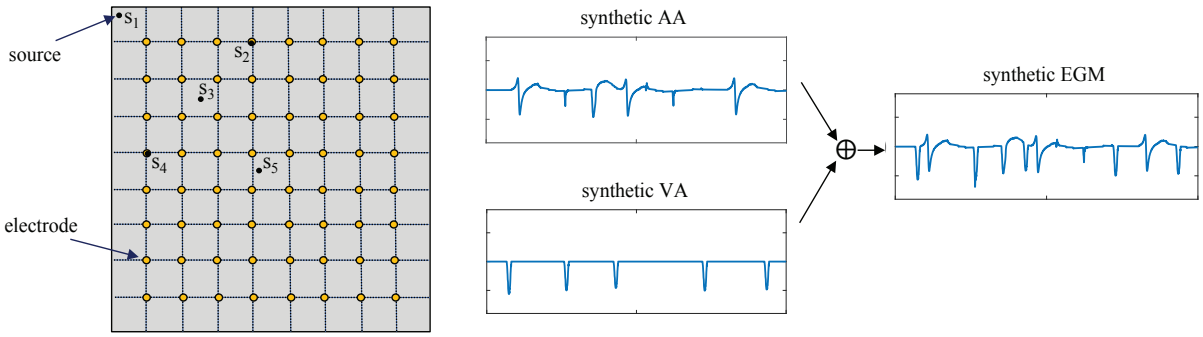

Figure 6: Simulation set up and synthetic signals during atrial fibrillation. *Left*: simulated two-dimensional tissue with 8×8 electrodes on top of it. Five foci sources s_1 to s_5 initiate the atrial fibrillation. *Right*: An example of synthetic atrial activity (AA), ventricular activity (VA), and mixed epicardial electrogram (EGM) with an atrial cycle length of 160 ms.

After generating the atrial activity, the next step was to generate the ventricular activity. The ventricular morphology was obtained by cutting out the ventricular segment in a heart beat during real sinus rhythm [40]. We inserted local variations in the amplitude and width of the different ventricular segments. Finally, we added the ventricular activity to the synthetic atrial activity to generate the mixed EGM.

Given the high computational complexity of these simulations, we considered an array of only 8×8 electrodes with the same inter-electrode spacing as the mapping array in Figure 1. The array is put on the tissue to measure the atrial EGM. The atrial EGM $\Phi(\mathbf{z}, t)$ measured by the electrode at location $\mathbf{z}$ at time t is calculated by [47]

$$\Phi(\mathbf{z}, t) = \frac{1}{4\pi\sigma_e} \int \frac{I_{\text{tm}}}{||\mathbf{z} - \mathbf{x}||} \mathrm{d}\mathbf{x} \tag{22}$$

where $\mathbf{z}$ and $\mathbf{x}$ represent the location vectors of the electrode and the cell, respectively, and σ_e is the extra-cellular conductivity.

6.2. Performance metrics

In the synthetic data scenario, we compared the estimated atrial activity with the pure atrial activity in terms of the normalized mean square error (NMSE) and the cross-correlation coefficient (CC). The NMSE is defined as

$$\text{NMSE} = \frac{1}{K} \sum_{i=1}^{K} \left(\frac{\sum_{t=0}^{T-1} (a_i(t) - a_i'(t))^2}{\sum_{t=0}^{T-1} (a_i(t))^2} \right) \tag{23}$$

where T is the length of the estimated atrial signal in the time domain, $a_i(t)$ and $a_i'(t)$ are the pure and the estimated atrial signals of the ith electrode at time t, respectively. The NMSE measures the normalized difference between the pure and the estimated atrial signals averaged over K electrodes: a lower value indicates a better estimation.

The cross-correlation coefficient is defined as

$$\text{CC} = \frac{1}{K} \sum_{i=1}^{K} \left(\frac{\sum_{t=0}^{T-1} \left(a_i(t) - \bar{a}_i\right) \left(a_i'(t) - \bar{a}_i'\right)}{\sqrt{\sum_{t=0}^{T-1} \left(a_i(t) - \bar{a}_i\right)^2} \sqrt{\sum_{t=0}^{T-1} \left(a_i'(t) - \bar{a}_i'\right)^2}} \right) \tag{24}$$

where $\bar{a}_i$ and $\bar{a}_i'$ are the mean of the true atrial signals and the mean of the estimated atrial signals of the ith electrode, respectively. The CC measures the similarity between the pure and the estimated atrial signals averaged over K electrodes: it is close to one if the pure and estimated atrial activities are correlated, and it is close to zero otherwise.

When using real data, it is impossible to use intrusive measures and quantify the performance through NMSE and CC since the ground truth is unknown. Hence, we use two non-intrusive metrics, namely: the ventricular depolarization reduction (VDR) [29], which measures the amplitude reduction of the R-peak; and the ventricular residue (VR) similar to [48], which considers both the area and the amplitude of the QRS[1] interval in the atrial activity.

For an EGM containing Q ventricular segments, the amplitude reduction of the R-peaks averaged over K electrodes is

$$\text{VDR} = \frac{1}{K} \sum_{i=1}^{K} \left(\frac{1}{Q} \sum_{q=1}^{Q} 10\log \left(\frac{R_{i,q}^{\text{m}}}{R_{i,q}'} \right) \right) \tag{25}$$

where $R_{i,q}^{\text{m}}$ is the qth R-peak amplitude of the mixed EGM (in the time domain) of the ith electrode, and $R_{i,q}'$ is the amplitude of the respective residue. A higher value of VDR indicates more reduction of the ventricular activity.

For an EGM containing Q ventricular activity segments, the averaged VR is

$$\text{VR} = \frac{1}{K} \sum_{i=1}^{K} \left(\frac{1}{Q} \sum_{q=1}^{Q} \left(\frac{A_{i,q} \sqrt{\sum_{t=b_{i,q}}^{e_{i,q}} \left(a_i'(t)\right)^2}}{\sqrt{\frac{1}{T} \sum_{t=0}^{T} \left(a_i(t)\right)^2}} \right) \right) \tag{26}$$

where $[b_{i,q}, e_{i,q}]$ is the qth QRS interval in the estimated atrial activity of the ith electrode, and $A_{i,q}$ is the maximum amplitude in this interval. A lower value of VR indicates a better extracted atrial activity.

[1] QRS is the combination of three graphical deflections (Q wave, R wave, and S wave) on a typical electrocardiogram.

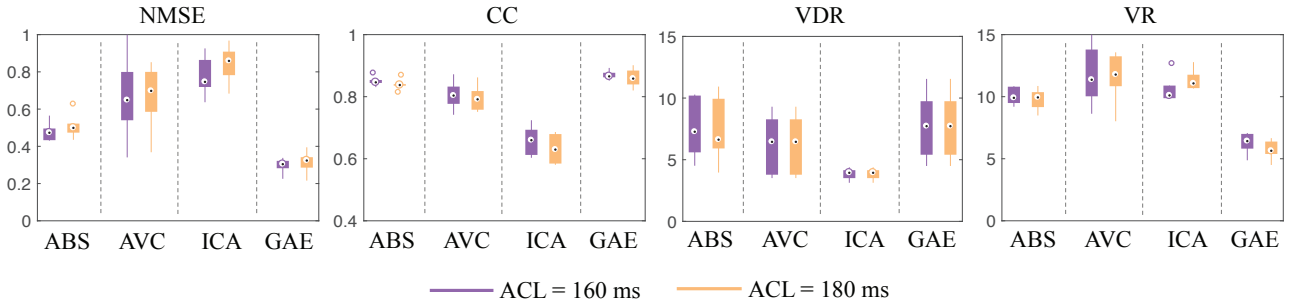

Figure 7: Boxplot performance on synthetic data of the average beat subtraction (ABS) [28], adaptive ventricular cancellation (AVC) [29], independent component analysis (ICA) [29], and the proposed graph-based atrial activity extraction (GAE) method. Two atrial cycle length (ACL) of 160 ms and 180 ms are considered. The proposed GAE method achieves the lowest normalized mean square error (NMSE) and ventricular residue (VR), and highest correlation coefficient (CC) and depolarization reduction (VDR) in both cases. The boxplots of NMSE, CC, and VR for the GAE method are comparatively short, which suggest that the GAE performance is more stable. Similar condensed boxplots are also observed for the ABS, but it presents outliers in the plots of NMSE and CC.

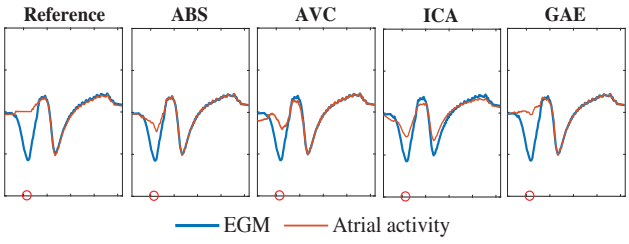

Figure 8: Illustrative example of the synthetic epicardial electrogram (EGM), synthetic pure atrial activity (AA) and the estimated atrial activity by the different algorithms. The left plot shows the synthetic EGM (blue) and the synthetic atrial activity (red). The other plots show the synthetic EGM (blue) and the estimated atrial activity (red) with different algorithms: average beat subtraction (ABS) [28]; adaptive ventricular cancellation (AVC) [29]; independent component analysis (ICA) [29]; proposed graph-based atrial activity extraction (GAE). The red circles mark the peak of the ventricular activity determined by the ECG measurements.

Table 1
Comparison of different algorithms for different patients during atrial fibrillation

Patient No.	Metrics	ABS	AVC	ICA	GAE
P1	VDR	11.06 (3.31)	7.99 (4.87)	5.68 (5.39)	**17.15 (6.31)**
	VR	3.66 (2.08)	7.86 (2.89)	10.24 (1.84)	**1.47 (0.50)**
P2	VDR	10.09 (3.43)	7.96 (2.76)	6.37 (4.85)	**16.98 (4.40)**
	VR	2.93 (0.80)	8.16 (1.66)	6.60 (2.58)	**1.19 (0.31)**
P3	VDR	11.41 (4.26)	7.80 (3.67)	8.55 (4.42)	**15.68 (4.34)**
	VR	3.17 (0.74)	7.08 (1.42)	6.71 (1.65)	**1.64 (0.58)**
P4	VDR	15.02 (4.12)	9.55 (4.27)	7.42 (4.06)	**16.85 (3.43)**
	VR	4.20 (0.50)	9.40 (2.21)	6.69 (1.35)	**1.80 (0.46)**
P5	VDR	7.80 (3.26)	8.73 (4.76)	6.59 (4.26)	**14.51 (3.57)**
	VR	5.07 (0.67)	8.94 (3.28)	10.20 (1.98)	**2.65 (0.46)**
P6	VDR	9.84 (2.97)	8.39 (4.20)	5.84 (1.67)	**16.57 (4.39)**
	VR	6.74 (1.14)	12.37 (2.88)	7.30 (1.67)	**2.43 (0.53)**
P7	VDR	10.39 (4.21)	6.86 (5.33)	4.34 (1.63)	**12.18 (4.64)**
	VR	3.03 (0.79)	9.43 (1.99)	12.44 (2.16)	**2.39 (0.68)**
P8	VDR	5.72 (3.91)	5.27 (3.55)	5.94 (2.46)	**11.95 (2.94)**
	VR	4.36 (0.57)	8.59 (1.81)	12.40 (1.53)	**2.60 (0.66)**
P9	VDR	14.59 (4.62)	7.71 (4.35)	4.53 (3.79)	**17.13 (5.54)**
	VR	**2.18 (0.74)**	12.70 (1.76)	13.21 (4.53)	2.62 (0.76)
P10	VDR	9.52 (4.57)	8.69 (5.05)	8.45 (4.25)	**14.93 (5.01)**
	VR	5.49 (0.74)	8.83 (3.33)	6.18 (2.09)	**2.14 (0.94)**
Mean	VDR	10.55 (4.85)	7.90 (5.01)	6.30 (4.26)	**15.39 (4.92)**
	VR	4.08 (1.63)	9.34 (2.54)	9.20 (1.12)	**2.09 (0.79)**

6.3. Results

Results on synthetic data: We evaluated the performance on the six segments for different degrees of atrial fibrillation. Figure 7 compares the proposed GAE algorithm with the reference methods. The performance of the GAE algorithm [cf. (18)] depends on the parameters c and μ. These parameters are chosen based on a grid search by minimizing the NMSE and are set to $c = 0.14$ and $\mu = 2$. We observe the proposed GAE method outperforms the other alternatives by achieving the smallest NMSE and VR, and the largest CC and VDR for both degrees of atrial fibrillation. The ABS performs worse since it cannot adapt to changes in the EGM morphology caused by the heart activity variations. The performance of the AVC is unstable because it relies on the reference signal. The ICA performs poorly on this data since the independence assumption between the atrial and ventricular activities might not always hold in the EGM data.

To further illustrate the differences of these methods, we show in Figure 8 an arbitrary example of the synthetic EGM, the ground truth atrial activity, and the estimated atrial activity. We see the signal extracted by the GAE method approximates the ground truth better than the comparative algorithms. The ABS algorithm performs also well, but leaves more ventricular components compared to the GAE method. Also, the AVC and the ICA algorithms face difficulties in annihilating the ventricular component.

Results on real data: We move now on to the results on the clinical EGMs. We evaluated the performance only through the non-intrusive metrics VDR [cf. (25)] and VR [cf. (26)]. Table 1 groups the results for the ten patients. For each patient, it reports the averaged performance over all electrodes and the respective standard deviation (in brackets). We see an improved performance of the proposed GAE algorithm further corroborated with the real data.

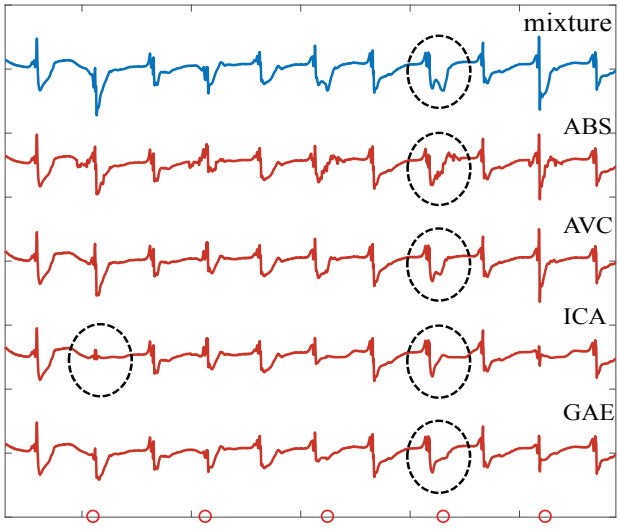

Figure 9: Illustrative example of the clinical epicardial electrogram (EGM) (blue) and the extracted atrial activity (red) by different algorithms: average beat subtraction (ABS) [28]; adaptive ventricular cancellation (AVC) [29]; independent component analysis (ICA) [29]; proposed graph-based atrial activity extraction (GAE). The proposed GAE method has less fluctuations and distortions and removes more ventricular activity.

Figure 9 shows a random example of the measured EGM and the extracted atrial activity by the different algorithms. The proposed GAE method extracts a smoother signal and has less ventricular component left. The extracted signal by ABS presents more fluctuations since ABS uses a fixed template to subtract the ventricular activity. The AVC shows a slightly better result than ABS, but it has more ventricular components left. The ICA can remove the ventricular activity well but fails in preserving the atrial activity.

6.4. Computational complexity & Implementation

The computational complexity of the GAE algorithm depends on the matrix inversion in (18). In each time frame and temporal frequency, the complexity is $\mathcal{O}(K^3)$, where K is the number of vertices (electrodes). For a signal with M time frames and T_M temporal frequencies, the computational complexity is $\mathcal{O}(M \times T_M \times K^3)$. This complexity is governed by the number of electrodes K in the array. For an array with large number of electrodes, the matrix inversion can be solved with the efficient conjugate gradient method to reduce the costs [49, 50].

For experiments, we implemented the GAE algorithm with MATLAB in an office laptop with 2.9 GHz Intel Core i5 processor and 8 GB RAM memory. The average run time for a segment of 10 s of data is around 1 s. The code for GAE algorithm is available at https://github.com/MiaoSGit/GAE. We remark that for the computation, improvements can be achieved with a coding in C, but this goes beyond the scope of this work.

7. Discussion and Future Recommendations

We proposed an approach based on graph signal processing to analyze atrial fibrillation. This method combines the graph Fourier transform with the short-time Fourier transform to analyze multi-electrode epicardial electrograms in a joint space, time, and frequency domain. By working with a higher-level model, we tackled the difficulties of analyzing the disease through complicated physical models. We found a strong link between the spatial and temporal variation of the atrial signal; and the atrial fibrillation reduces the signal spatial variation. We also characterized the space-time-frequency differences of the atrial and ventricular activities and developed a graph-based algorithm to estimate the atrial signal from the mixed measurements. The proposed algorithm corroborates our theory by showcasing improved performance with respect to other state-of-the-art methods.

The proposed framework has also limitations. An initial difficulty we faced is how to construct the most representative graph. While we relied on a Euclidean-based nearest neighbor approach, it remains still an open question whether it is possible to find a more meaningful structure through graph learning techniques [51]. The graph is, in fact, crucial since it gives the Fourier basis to capture the spatial variability. We believe the performance of the graph-based extraction algorithm can be improved substantially if smooth-based graphs are learned [52, 53]. Among the same lines, it remains unanswered whether directed graphs and other graph representation matrices (e.g., normalized or random walk Laplacian) can yield different insights on atrial fibrillation.

It did not escape our notice that the graph-based extraction algorithm imposes a tradeoff between the preservation of the atrial activity and the reduction of the ventricular activity. The latter is heavily influenced by the smoothness upper-bound in (19). This parameter along with the Lagrange penalty term has been selected using a grid search. However, it deserves further investigation to check if constant values for different patients are a good choice or if we need to adjust the values for each separate case. We also believe that other graph- and graph-time priors such as diffusion or bandlimitedness can impose a better tradeoff for atrial activity extraction [54, 55].

Another direction worth taking in the near future is to corroborate our findings on a larger dataset, with induced and spontaneous atrial fibrillation, and to characterize the graph-time spectral behavior of the disease levels. In this direction, we also aim to adopt graph-based techniques to detect atrial fibrillation triggers from electrogram measurements.

Altogether, our aim is to raise attention to explore spatial-temporal spectral properties of electrocardiograms to move forward the research of atrial fibrillation.

8. Conclusions

We suggested a new approach to study the epicardial electrograms for atrial fibrillation. This approach relies on

graph signal processing–a recent research area in the signal processing community–to model electrograms during atrial fibrillation with a higher level model. We conducted a novel graph-time spectral analysis study to analyze the epicardial electrograms in the joint space, time, and frequency domains. We found the spatial variation is related to the high temporal variation; precisely, a faster temporal variation induces a high spatial variation. We also found that the atrial fibrillation reduces the high temporal frequencies of the atrial electrogram. Together, these observations suggest that atrial fibrillation decreases the spatial variation of the atrial activity. We also observed the ventricular activity is smoother over the graph compared with the atrial activity. In this respect, we designed a graph-based atrial activity extraction algorithm that leverages the smoothness prior to estimate the atrial activity. Our experimental results with synthetic data and real electrocardiograms showed the propose method outperforms reference methods based on average beat subtraction, adaptive ventricular cancellation and independent component analysis. These findings shed light to new ways to approach the disease and may be of help to further understand its mechanisms.

References

[1] C. T. January, et al., 2014 AHA/ACC/HRS guideline for the management of patients with atrial fibrillation: A report of the American College of Cardiology/American Heart Association Task Force on Practice Guidelines and the Heart Rhythm Society, Journal of the American College of Cardiology 64 (21) (2014) e1–e76.

[2] P. S. J. Miller, et al., Are cost benefits of anticoagulation for stroke prevention in atrial fibrillation underestimated?, Stroke 36 (2) (2005) 360–366.

[3] Y. Miyasaka, et al., Mortality trends in patients diagnosed with first atrial fibrillation: A 21-year community-based study, Journal of the American College of Cardiology 49 (9) (2007) 986–992.

[4] T. Nitta, et al., Concurrent multiple left atrial focal activations with fibrillatory conduction and right atrial focal or reentrant activation as the mechanism in atrial fibrillation, The Journal of Thoracic and Cardiovascular Surgery 127 (3) (2004) 770–778.

[5] V. Barbaro, P. Bartolini, G. Calcagnini, F. Censi, S. Morelli, A. Michelucci, Mapping the organization of atrial fibrillation with basket catheters part i: Validation of a real-time algorithm, Pacing and Clinical Electrophysiology 24 (7) (2001) 1082–1088.

[6] G. Calcagnini, F. Censi, A. Michelucci, P. Bartolini, Descriptors of wavefront propagation, IEEE Engineering in Medicine and Biology Magazine 25 (6) (2006) 71–78.

[7] V. Barbaro, P. Bartolini, G. Calcagnini, F. Censi, A. Michelucci, Measure of synchronisation of right atrial depolarisation wavefronts during atrial fibrillation, Medical and Biological Engineering and Computing 40 (1) (2002) 56–62.

[8] C. P. Teuwen, C. Kik, L. J. van der Does, E. A. Lanters, P. Knops, E. M. Mouws, A. J. Bogers, N. M. de Groot, Quantification of the arrhythmogenic effects of spontaneous atrial extrasystole using high-resolution epicardial mapping, Circulation: Arrhythmia and Electrophysiology 11 (1) (2018) e005745.

[9] T. H. Everett, L.-C. Kok, R. H. Vaughn, R. Moorman, D. E. Haines, Frequency domain algorithm for quantifying atrial fibrillation organization to increase defibrillation efficacy, IEEE Transactions on Biomedical Engineering 48 (9) (2001) 969–978.

[10] V. Jacquemet, et al., Analysis of electrocardiograms during atrial fibrillation, IEEE Engineering in Medicine and Biology Magazine 25 (6) (2006) 79–88.

[11] A. Bollmann, et al., Frequency analysis of human atrial fibrillation using the surface electrocardiogram and its response to ibutilide, The American Journal of Cardiology 81 (12) (1998) 1439–1445.

[12] Q. Xi, et al., Atrial fibrillatory wave characteristics on surface electrogram: ECG to ECG repeatability over twenty-four hours in clinically stable patients, Journal of Cardiovascular Electrophysiology 15 (8) (2004) 911–917.

[13] R. P. Houben, et al., Analysis of fractionated atrial fibrillation electrograms by wavelet decomposition, IEEE Transactions on Biomedical Engineering 57 (6) (2010) 1388–1398.

[14] M. Brandstein, D. Ward, Microphone arrays: Signal processing techniques and applications, Springer Science & Business Media, 2013.

[15] V. D. van Veen, K. M. Buckley, Beamforming: a versatile approach to filtering, IEEE ASSP Magazine 5 (2) (1988) 4–24.

[16] D. M. Lombardo, et al., Comparison of detailed and simplified models of human atrial myocytes to recapitulate patient specific properties, PLoS Computational Biology 12 (8) (2016).

[17] M. Newman, Networks, Oxford university press, 2018.

[18] W. Huang, et al., Graph frequency analysis of brain signals, IEEE Journal of Selected Topics in Signal Processing 10 (7) (2016) 1189–1203.

[19] J. D. Medaglia, et al., Functional alignment with anatomical networks is associated with cognitive flexibility, Nature Human Behaviour 2 (2) (2018) 156–164.

[20] W. Huang, et al., A graph signal processing perspective on functional brain imaging, Proceedings of the IEEE 106 (5) (2018) 868–885.

[21] C. Hu, et al., Matched signal detection on graphs: Theory and application to brain imaging data classification, NeuroImage 125 (2016) 587–600.

[22] E. Isufi, A. S. Mahabir, G. Leus, Blind graph topology change detection, IEEE Signal Processing Letters 25 (5) (2018) 655–659.

[23] H. Behjat, N. Leonardi, L. Sörnmo, D. V. D. Ville, Anatomically-adapted graph wavelets for improved group-level fmri activation mapping, NeuroImage 123 (2015) 185–199.

[24] Y. Guo, H. Nejati, N. Cheung, Deep neural networks on graph signals for brain imaging analysis, in: IEEE International Conference on Image Processing (ICIP), IEEE, 2017, pp. 3295–3299.

[25] A. Yaksh, et al., A novel intra-operative, high-resolution atrial mapping approach, Journal of Interventional Cardiac Electrophysiology 44 (3) (2015) 221–225.

[26] L. Sun, et al., A preliminary study on atrial epicardial mapping signals based on graph theory, Medical Engineering & Physics 36 (7) (2014) 875–881.

[27] S. Aliaksei, M. F. M. José, Big data analysis with signal processing on graphs: Representation and processing of massive data sets with irregular structure, IEEE Signal Processing Magazine 31 (5) (2014) 80–90.

[28] J. Slocum, et al., Computer detection of atrioventricular dissociation from surface electrocardiograms during wide QRS complex tachycardias, Circulation 72 (5) (1985) 1028–1036.

[29] J. J. Rieta, F. Hornero, Comparative study of methods for ventricular activity cancellation in atrial electrograms of atrial fibrillation, Physiological Measurement 28 (8) (2007) 925–936.

[30] D. Raine, P. Langley, A. Murray, S. S. Furniss, J. P. Bourke, Surface atrial frequency analysis in patients with atrial fibrillation: assessing the effects of linear left atrial ablation, Journal of Cardiovascular Electrophysiology 16 (8) (2005) 838–844.

[31] J. J. Rieta, F. Castells, C. Sánchez, V. Zarzoso, J. Millet, Atrial activity extraction for atrial fibrillation analysis using blind source separation, IEEE Transactions on Biomedical Engineering 51 (7) (2004) 1176–1186.

[32] P. Langley, et al., Comparison of atrial signal extraction algorithms in 12-lead ECGs with atrial fibrillation, IEEE Transactions on Biomedical Engineering 53 (2) (2006) 343–346.

[33] M. J. van Campenhout, et al., Bachmann's bundle: A key player in the development of atrial fibrillation?, Circulation: Arrhythmia and Electrophysiology 6 (5) (2013) 1041–1046.

[34] L. J. van der Does, A. Yaksh, C. Kik, P. Knops, E. A. Lanters, C. P. Teuwen, et al., Quest for the arrhythmogenic substrate of atrial fibril-

lation in patients undergoing cardiac surgery (quasar study): rationale and design, Journal of Cardiovascular Translational Research 9 (3) (2016) 194–201.

[35] E. A. Lanters, D. M. van Marion, C. Kik, H. Steen, A. J. Bogers, M. A. Allessie, B. J. Brundel, N. M. de Groot, HALT & REVERSE: Hsf1 activators lower cardiomyocyt damage; towards a novel approach to reverse atrial fibrillation, Journal of Translational Medicine 13 (1) (2015) 347.

[36] D. I. Shuman, et al., The emerging field of signal processing on graphs: Extending high-dimensional data analysis to networks and other irregular domains, IEEE Signal Processing Magazine 30 (3) (2013) 83–98.

[37] J. J. Rieta, et al., Atrial activity extraction based on blind source separation as an alternative to QRST cancellation for atrial fibrillation analysis, in: Computers in Cardiology, 2000, pp. 69–72.

[38] M. Stridh, L. Sornmo, Spatiotemporal QRST cancellation techniques for analysis of atrial fibrillation, IEEE Transactions on Biomedical Engineering 48 (1) (2001) 105–111.

[39] F. Castells, et al., Spatiotemporal blind source separation approach to atrial activity estimation in atrial tachyarrhythmias, IEEE Transactions on Biomedical Engineering 52 (2) (2005) 258–267.

[40] F. Castells, et al., Atrial fibrillation analysis based on ICA including statistical and temporal source information, in: IEEE International Conference on Acoustics, Speech, and Signal Processing, 2003, pp. V–94–96.

[41] V. D. Corino, M. W. Rivolta, R. Sassi, F. Lombardi, L. T. Mainardi, Ventricular activity cancellation in electrograms during atrial fibrillation with constraints on residuals' power, Medical Engineering & Physics 35 (12) (2013) 1770–1777.

[42] M. Haissaguerre, P. Jaïs, D. C. Shah, A. Takahashi, M. Hocini, G. Quiniou, S. Garrigue, A. L. Mouroux, P. L. Métayer, J. Clémenty, Spontaneous initiation of atrial fibrillation by ectopic beats originating in the pulmonary veins, New England Journal of Medicine 339 (10) (1998) 659–666.

[43] P. Ganesan, K. E. Shillieto, B. Ghoraani, Simulation of spiral waves and point sources in atrial fibrillation with application to rotor localization, in: 2017 IEEE 30th International Symposium on Computer-Based Medical Systems (CBMS), IEEE, 2017, pp. 379–384.

[44] M. R. Courtemanche, R. J. Ramirez, S. Nattel, Ionic mechanisms underlying human atrial action potential properties: insights from a mathematical model, American Journal of Physiology-Heart and Circulatory Physiology 275 (1) (1998) H301–H321.

[45] M. Courtemanche, R. J. Ramirez, S. Nattel, Ionic targets for drug therapy and atrial fibrillation-induced electrical remodeling: insights from a mathematical model, Cardiovascular Research 42 (2) (1999) 477–489.

[46] R. Plonsey, R. C. Barr, Bioelectricity: a quantitative approach, Springer Science & Business Media, 2007.

[47] N. Virag, et al., Study of atrial arrhythmias in a computer model based on magnetic resonance images of human atria, Chaos: An Interdisciplinary Journal of Nonlinear Science 12 (3) (2002) 754–763.

[48] R. Alcaraz, J. J. Rieta, Adaptive singular value cancelation of ventricular activity in single-lead atrial fibrillation electrocardiograms, Physiological Measurement 29 (12) (2008) 1351.

[49] J. R. Shewchuk, An introduction to the conjugate gradient method without the agonizing pain (1994).

[50] J. Liu, E. Isufi, G. Leus, Filter design for autoregressive moving average graph filters, IEEE Transactions on Signal and Information Processing over Networks 5 (1) (2018) 47–60.

[51] G. Mateos, S. Segarra, A. G. Marques, A. Ribeiro, Connecting the dots: Identifying network structure via graph signal processing, IEEE Signal Processing Magazine 36 (3) (2019) 16–43.

[52] V. Kalofolias, How to learn a graph from smooth signals, in: Artificial Intelligence and Statistics, 2016, pp. 920–929.

[53] K. Qiu, et al., Time-varying graph signal reconstruction, IEEE Journal of Selected Topics in Signal Processing 11 (6) (2017) 870–883.

[54] A. G. Marques, et al., Stationary graph processes and spectral estimation, IEEE Transactions on Signal Processing 65 (22) (2017) 5911–5926.

[55] N. Perraudin, et al., Towards stationary time-vertex signal processing, in: IEEE International Conference on Acoustics, Speech and Signal Processing, 2017, pp. 3914–3918.